

# Numerical experiments on plasma focus neutron yield versus pressure compared with laboratory experiments

S Lee<sup>1,2,3</sup>, S H Saw<sup>1,2</sup>, L Soto<sup>1,4,5</sup>, S V Springham<sup>3</sup> and S P Moo<sup>1</sup>

<sup>1</sup> Institute for Plasma Focus Studies, 32 Oakpark Drive, Chadstone, VIC3148, Australia

<sup>2</sup> INTI University College, 71800 Nilai, Malaysia

<sup>3</sup> National Institute of Education, Nanyang Technological University, Singapore 637616, Singapore

<sup>4</sup> Comisión Chilena de Energía Nuclear, Casilla 188-D, Santiago, Chile

<sup>5</sup> Center for Research and Applications in Plasma Physics and Pulsed Power, P<sup>4</sup>, Santiago-Curicó, Chile

E-mail: [leesing@optusnet.com.au](mailto:leesing@optusnet.com.au)

Received 21 February 2009, in final form 16 April 2009

Published 19 May 2009

Online at [stacks.iop.org/PPCF/51/075006](http://stacks.iop.org/PPCF/51/075006)

## Abstract

Published literature shows that the neutron yield of the plasma focus has been modeled in two papers using a thermonuclear mechanism. However, it is more widely held that plasma focus neutrons are produced mainly by non-thermalized mechanisms such as beam–target. Moreover these papers use several parameters which are adjusted for each machine until the computed neutron yield  $Y_n$  data agree with measured  $Y_n$  data. For this paper numerical experiments are carried out, using the Lee model code, incorporating a beam–target mechanism to compute the  $Y_n$  versus pressure data of plasma focus devices PF-400 J and FN-II. The Lee model code is first configured for each of these two machines by fitting the computed current waveform against a measured current waveform. Thereafter all results are computed without adjusting any parameters. Computed results of  $Y_n$  versus pressure for each device are compared with the measured  $Y_n$  versus pressure data. The comparison shows degrees of agreement between the laboratory measurements and the computed results.

## 1. Introduction

The dense plasma focus produces copious multi-radiation, including a wide spectrum of photons and particles, which is the subject of many studies and applications. From many devices and experiments have been gathered a large array of data and information leading to interesting discussions. For example, to explain the observed fast particles with energies up to megaelectronvolt emitted from devices operating at tens of kilovolts, mechanisms such

as micro-instabilities, magnetohydrodynamic instabilities, acceleration by turbulence and ‘anomalous’ plasma resistance have been postulated [1, 2]. Working with these ideas enables some numbers to be estimated regarding, for example, beam particle energies.

One of the most important emissions of the plasma focus is the fusion neutrons, which for a deuterium focus derive from the D–D fusion reaction, resulting in 2.45 MeV neutrons. Much data have been accumulated experimentally including pulse duration and time characteristics of emission, neutron spectra and spatial anisotropy of emission and yields [1]. From these data, scaling rules of neutron yield  $Y_n$  versus storage energy  $E_0$  or discharge current,  $I$ , have been deduced. The yield  $Y_n$  was found to be much higher than could be from thermonuclear reactions, given the measured parameters of the plasma focus pinch. Mechanisms such as moving boiler, beam–target, gyrating particles [1–5] and others such as quasi-Maxwellian hot plasmoids [6] have been invoked to explain the high measured  $Y_n$ . These neutron generating mechanisms are assumed to be consequential to the instabilities, etc discussed in the last paragraph. Again from such mechanisms come forth general results such as the temporal and spatial characteristics of the neutron pulses, and representative yield numbers put forward to illustrate the validity of the assumed mechanism. There do not appear to be any published results demonstrating non-thermonuclear modeling which may be applied to any particular machine to derive  $Y_n$  in a manner where such modeled data may be compared with specific experiments.

Given that it is widely held that the neutron yield from the plasma focus is predominantly from non-thermonuclear mechanisms [1–5] it is interesting that model codes have been developed using a thermonuclear mechanism that claim to have achieved agreement with laboratory measurements for  $Y_n$  data [7, 8]. It may be commented that both these papers use parameters such as axial sweeping and radial sweeping efficiency factors which are adjusted until the computed  $Y_n$  data agree with the measured  $Y_n$  data. Moreover, the kind of temperatures needed in the computation for the gross pinch (as distinct from hot spots), several kiloelectronvolts, is unlikely to be achieved in the actual plasma focus pinch. Specifically it may be commented that figure 16 of Gonzalez *et al* [8] shows a computed peak radial speed of  $72 \text{ cm } \mu\text{s}^{-1}$ , which is a factor of at least 2 higher than that observed experimentally for typical neutron optimized operation [1, 2]. Such a speed generates, in a deuterium plasma, as can be shown from shock equations, a temperature of 2.1 keV, which is 4 times higher than that computed were the speed to be half the claimed value. The reflected shock raises the temperature further to 5 keV, and then follows the pinch compression raising the temperature still higher. In this range of temperature, a factor of 4 in temperature gives a factor  $\sim 1000$  times in the thermalized D–D fusion cross-section [9]. One might wish to ponder how their modeling gives such unrealistically high temperatures.

Reference [8] states that in their model, the ‘kinematics’ of the current sheet follows Lee’s model, quoting [10], of 1983 vintage. A critical problem of the Lee model code, versions up to 1995, was that the computed speeds of the radial phase were too high by a factor of about 2. The modeling of the radial phase considers an imploding slug (of plasma) the front of which is a shock wave and the rear of which is the magnetic piston driving the imploding shock front. In modeling such an imploding slug, there is an implicit assumption that the shock front and the magnetic piston are in instantaneous communication. It was pointed out by Potter [11] that the non-infinite speed of small disturbances means that as the axis is approached, the communication delay between the front and the back of the slug becomes significant. When this communication delay was implemented into the Lee model code [12, 13] the modeled speeds reduced by a factor of about 2 and became more realistic when compared with experimental observations. This critical feature, of a ‘signal-delay slug’ has since been built into every version of the Lee model code [12, 13].

The imploding radial layer modeled by [8] does not have this vital 'signal-delay' mechanism, and thus ends up computing unrealistic high speeds (factor of 2 too high), which would lead to equally unrealistic high temperatures (factor of 4 too high; hence a factor of  $\sim 1000$  times too high in thermonuclear fusion cross-section) in their modeling of the pinch compression phase. Without this unrealistically modeled high speeds it is doubtful that even the most extreme adjustments of the sweeping factors would enable agreement of the computed thermonuclear  $Y_n$  with the measured  $Y_n$ .

Recently, the Lee model code was equipped with a beam-target mechanism which computes the  $Y_n$  for a wide range of plasma focus machines ranging from the sub-kilojoule PF-400 J to the megajoule PF1000. The computed yields are typically within a factor of 2 compared with the measured  $Y_n$  [14, 15]. Numerical experiments using this code over a wide range of plasma focus machines and energies have derived scaling rules of  $Y_n$ .

In this paper we show that the Lee model code is not only able to compute  $Y_n$  for various machines but that it is able to compute data such as  $Y_n$  versus  $P_0$ . We choose two specific machines the PF-400 J [16] and FN-II [17] (Fuego Nuevo II) which have well-documented published data on  $Y_n$  versus  $P_0$  as well as sufficient published machine parameters and measured current traces, so that numerical experiments may be carried out with the Lee model code. The computed  $Y_n$  versus  $P_0$  curve in each case is compared with the published measured  $Y_n$  versus  $P_0$  data.

The Lee model couples the electrical circuit with plasma focus dynamics, thermodynamics and radiation, enabling realistic simulation of all gross focus properties. The basic model, described in 1984 [10], was successfully used to assist several experiments [18–21]. Radiation-coupled dynamics was included in the five-phase code leading to numerical experiments on radiation cooling [22]. The signal-delay slug, so crucial to radial simulation, was incorporated together with real gas thermodynamics and radiation-yield terms and assisted other research projects [23, 25, 26] and was web-published in 2000 [12] and 2005 [13]. All subsequent versions of the Lee model code incorporate the 'signal-delay slug' as a must-have feature. Plasma self-absorption was included in 2007 [12], improving soft x-ray yield simulation. The code has been used extensively in several machines including UNU/ICTP PFF [18, 21–24], NX2 [25, 26] NX1 [25], and adapted for the Filippov-type plasma focus DENA [27]. A recent development is the inclusion of neutron yield,  $Y_n$ , using a beam-target mechanism [3], incorporated in the present version [28] of the code RADPFV5.13.b (and later versions), resulting in realistic  $Y_n$  scaling with  $I_{\text{pinch}}$  [14, 15]. The versatility and utility of the Lee model is demonstrated in its clear distinction of  $I_{\text{pinch}}$  from  $I_{\text{peak}}$  [29] and the recent uncovering of a plasma focus pinch current limitation effect [30, 31]. The description, theory, and up-to-date code and a broad range of results of this 'Universal Plasma Focus Laboratory Facility' are available for download [28].

The neutron yield is computed using a phenomenological beam-target neutron generating mechanism described recently by Gribkov *et al* [3] and adapted to yield the following equation. A beam of fast deuteron ions is produced by diode action in a thin layer close to the anode, with plasma disruptions generating the necessary high voltages. The beam interacts with the hot dense plasma of the focus pinch column to produce the fusion neutrons. The beam-target yield is derived [14, 15, 28, 31] as

$$Y_{\text{b-t}} = C_n n_i I_{\text{pinch}}^2 z_p^2 (\ln(b/r_p)) \sigma / U^{0.5},$$

where  $n_i$  is the ion density,  $b$  is the cathode radius,  $r_p$  is the radius of the plasma pinch with length  $z_p$ ,  $\sigma$  the cross-section of the D–D fusion reaction, n-branch [9] and  $U$ , the beam energy.  $C_n$  is treated as a calibration constant combining various constants in the derivation process.

The D–D cross-section is sensitive to the beam energy in the range 15–150 kV; so it is necessary to use the appropriate range of beam energy to compute  $\sigma$ . The code computes induced voltages (due to current motion inductive effects)  $V_{\max}$  of the order of only 15–50 kV. However it is known, from experiments that the ion energy responsible for the beam–target neutrons is in the range 50–150 keV [3], and for smaller lower voltage machines the relevant energy could be lower at 30–60 keV [5]. Thus in line with the experimental observations the D–D cross section  $\sigma$  is reasonably obtained by using  $U = 3V_{\max}$ . This fit was tested by using  $U$  equal to various multiples of  $V_{\max}$ . A reasonably good fit of the computed neutron yields to the measured published neutron yields at energy levels from sub-kilojoule to near megajoule was obtained when the multiple of 3 was used; with poor agreement for most of the data points when, for example, a multiple of 1 or 2 or 4 or 5 was used. The model uses a value of  $C_n = 2.7 \times 10^7$  obtained by calibrating the yield [28, 31] at an experimental point of 0.5 MA.

The thermonuclear component is also computed in every case and it is found that this component is negligible when compared with the beam–target component.

## 2. Procedures for the numerical experiments

The Lee model code is configured to work as any plasma focus by inputting the bank parameters,  $L_0$ ,  $C_0$  and stray circuit resistance  $r_0$ ; the tube parameters  $b$ ,  $a$  and  $z_0$  and operational parameters  $V_0$  and  $P_0$  and the fill gas. The standard practice is to fit the computed total current waveform to an experimentally measured total current waveform [12–15, 28–31] using four model parameters representing the mass swept-up factor  $f_m$ , the plasma current factor  $f_c$  for the axial phase and factors  $f_{mr}$  and  $f_{cr}$  for the radial phases. The mass swept-up factor  $f_m$  accounts for not only the porosity of the current sheet but also for the inclination of the moving current sheet–shock front structure, contact layers and all other unspecified mechanisms which have effects equivalent to increasing or reducing the amount of mass in the moving structure, during the axial phase. The current factor  $f_c$  accounts for the fraction of current effectively flowing in the moving structure (due to all effects such as current shedding at or near the back-wall and current sheet inclination). This defines the fraction of current effectively driving the structure, during the axial phase. Likewise the radial phase mass swept-up and current factors  $f_{mr}$  and  $f_{cr}$  are incorporated in all three radial phases. The mass swept-up factor  $f_{mr}$  accounts for all mechanisms which have effects equivalent to increasing or reducing the amount of mass in the moving slug, during the radial phase, not the least of which could be the ejection of mass in the axial direction. The current factor  $f_{cr}$  accounts for the fraction of current effectively flowing in the moving piston forming the back of the slug (due to all effects). This defines the fraction of current effectively driving the radial slug. The pinch current  $I_{\text{pinch}}$  is therefore obtained by multiplying the total (circuit) current at the time of pinch by  $f_{cr}$ .

From experience it is known that the current trace of the focus is one of the best indicators of gross performance. The axial and radial phase dynamics and the crucial energy transfer into the focus pinch are among the important information that is quickly apparent from the current trace.

The exact time profile of the total current trace is governed by the bank parameters, by the focus tube geometry and the operational parameters. It also depends on the fraction of mass swept-up and the fraction of sheath current and the variation of these fractions through the axial and radial phases. These parameters determine the axial and radial dynamics, specifically the axial and radial speeds which in turn affect the profile and magnitudes of the discharge current. The detailed profile of the discharge current during the pinch phase also reflects the Joule heating and radiative yields. At the end of the pinch phase the total current profile also reflects the sudden transition of the current flow from a constricted pinch to a large column

flow. Thus the discharge current powers all dynamic, electrodynamic, thermodynamic and radiation processes in the various phases of the plasma focus. Conversely all the dynamic, electrodynamic, thermodynamic and radiation processes in the various phases of the plasma focus affect the discharge current. It is then no exaggeration to say that the discharge current waveform contains information on all the dynamic, electrodynamic, thermodynamic and radiation processes that occur in the various phases of the plasma focus. This explains the importance attached to matching the computed current trace to the measured current trace in the procedure adopted by the Lee model code.

Once the current matching is done, and the model parameters are fixed, with adjustments to  $L_0$ ,  $C_0$ ,  $r_0$  and  $z_0$  as required by the current matching, all these parameters are fixed and no further adjustment is made to any of the bank, tube and model parameters.

It is observed in laboratory measurements that towards the end of the focus pinch phase plasma/current disruptions occur resulting in localized regions of high densities and temperatures. These localized regions are not modeled in the code, which consequently computes only an average uniform density and an average uniform temperature which are considerably lower than measured peak density and temperature. However, because the four model parameters are obtained by fitting the computed total current waveform to the measured total current waveform, the model incorporates the energy and mass balances equivalent, at least in the gross sense, to all the processes which are not even specifically modeled. Hence, computed gross features such as speeds and trajectories and integrated soft x-ray yields have been extensively tested in numerical experiments on several machines, and found to be comparable with the measured values. Although these current/plasma disruptions are not specifically modeled, as explained earlier, our beam–target mechanism for neutron production is based on such disruptions.

### 3. PF-400 J—the numerical experiments

#### 3.1. Fitting the computed current trace to obtain the model parameters

Silva *et al* had published a paper [16] with laboratory measurements from the PF-400 J, including a typical current waveform at 6.6 Torr deuterium, and a graph of neutron yield versus pressure. We first fit the computed current waveform to the published measured waveform [16] in the following manner.

We configure the Lee model code (version RADPF05.13.9b) to operate as the PF-400 J, starting with the following published [16] bank and tube parameters:

Bank parameters:  $L_0 = 38$  nH,  $C_0 = 0.88$   $\mu$ F,  $r_0 =$  not given

Tube parameters:  $b = 1.55$  cm,  $a = 0.6$  cm,  $z_0 = 2.8$  cm

Operating parameters:  $V_0 = 28$  kV,  $P_0 = 6.6$  Torr deuterium,

where  $L_0$  is the static inductance (nominal),  $C_0$  the storage capacitance (nominal),  $b$  the tube outer radius,  $a$  the inner radius,  $z_0$  the anode length,  $V_0$  the operating voltage and  $P_0$  the operating initial pressure.

The computed total discharge current waveform is fitted to the measured by varying model parameters  $f_m$ ,  $f_c$ ,  $f_{mr}$  and  $f_{cr}$  one by one until the computed waveform agrees with the measured waveform. First, the axial model factors  $f_m$ ,  $f_c$  are adjusted (fitted) until the computed rising slope of the total current trace and the rounding off of the peak current as well as the peak current itself are in reasonable (typically good) fit with the measured total current trace. Then we proceed to adjust (fit) the radial phase model factors  $f_{mr}$  and  $f_{cr}$  until the computed slope and depth of the dip agree with the measured. This procedure is quite

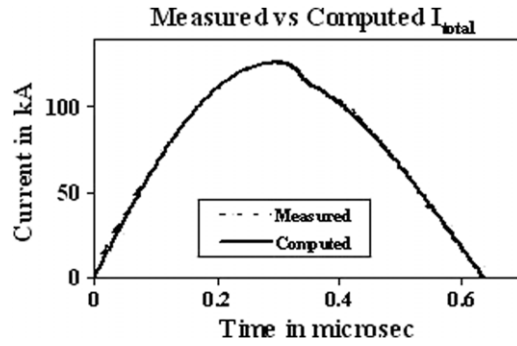


**Figure 1.** PF-400J: computed discharge current compared with the published measured current [16].

sensitive and robust in that if any bank parameter such as  $L_0$  or  $C_0$  is not correctly given, no good fit is obtainable (i.e. the computed total current trace will not be matchable with the measured waveform no matter how the four model parameters are varied).

In the case of PF-400 J, to obtain a reasonably good fit of the computed current waveform with the measured current waveform, the following bank and tube parameters ( $L_0$ ,  $C_0$  and  $z_0$  refitted and  $r_0$  fitted) have to be used:

Bank parameters:  $L_0 = 40$  nH,  $C_0 = 0.95$   $\mu$ F,  $r_0 = 10$  m $\Omega$

Tube parameters:  $b = 1.55$  cm,  $a = 0.6$  cm,  $z_0 = 1.7$  cm

Operating parameters:  $V_0 = 28$  kV,  $P_0 = 6.6$  Torr deuterium

together with the following fitted model parameters:

$$f_m = 0.08, \quad f_c = 0.7, \quad f_{mr} = 0.11 \quad \text{and} \quad f_{cr} = 0.7.$$

The fitted computed current waveform is compared with the published waveform in figure 1, showing good agreement, the two traces practically inseparable.

### 3.2. Computing the neutron yield as a function of operating pressure

The code is configured to operate as the PF-400J using the bank and tube parameters last mentioned above and using the fitted model parameters. Numerical experiments are then carried out at an operating voltage of 28 kV and at various initial pressures in deuterium. The neutron yields  $Y_n$  are then tabulated in Table 1 together with some of the computed properties of the focus pinch. The computed  $Y_n$  versus  $P_0$  curve is compared with the published data [16] in figure 2.

Figure 2 shows that the computed neutron yield versus pressure curve agrees reasonably with the published curve. The main features for comparison include the peak  $Y_n$  (computed value of  $1.16 \times 10^6$  against a measured value of  $1.06 \times 10^6$  neutrons per shot); optimum  $P_0$  (computed value of 6–7 mb against the measured value of 9 mb) and the drop-off of  $Y_n$  on both sides of the optimum, although the computed drop-offs are more gradual than the measured.

## 4. FN-II—the numerical experiments

### 4.1. Fitting the computed current trace to obtain the model parameters

Castillo *et al* published a paper [17] with laboratory measurements from the FN-II including a typical current derivative waveform and data on neutron yield flux (end-on and side-on)

**Table 1.** PF-400J: computed  $Y_n$  as a function of pressure, together with some computed pinch properties.  $I_{\text{peak}}$  is the peak value of the total current,  $I_{\text{pinch}}$  the plasma pinch current at start of pinch,  $T_{\text{pinch}}$  the pinch temperature,  $v_a$  the axial speed,  $v_s$ ,  $v_p$  the radial shock and piston speeds,  $r_{\text{min}}$  the minimum radius of focus,  $z_{\text{max}}$  the maximum length of pinch column, 'pinch dur' the pinch duration,  $V_{\text{max}}$  the maximum induced voltage and  $n_i$  the ion number density.

$P_0$ (mb)	$Y_n$ ( $10^6$ neutrons)	$I_{\text{peak}}$ (kA)	$I_{\text{pinch}}$ (kA)	Min $T_{\text{pinch}}$ ( $10^6$ )	Max $T_{\text{pinch}}$ ( $10^6$ )	Peak $v_a$ ( $\text{cm } \mu\text{s}^{-1}$ )	Peak $v_s$ ( $\text{cm } \mu\text{s}^{-1}$ )	Peak $v_p$ ( $\text{cm } \mu\text{s}^{-1}$ )	$r_{\text{min}}$ (cm)	$z_{\text{max}}$ (cm)	Pinch dur (ns)	$V_{\text{max}}$ (kV)	$n_i$ ( $10^{23} \text{ m}^{-3}$ )
15.0	0.27	127	70	2.5	2.7	7.0	23.5	16.0	0.09	0.8	8.0	9.3	6.18
14.0	0.38	127	73	2.9	3.1	7.3	24.8	16.9	0.09	0.8	7.5	10.3	5.95
13.0	0.50	127	75	3.3	3.5	7.5	26.3	17.8	0.09	0.8	7.0	11.4	5.70
12.0	0.64	127	77	3.8	4.0	7.8	27.9	18.8	0.09	0.8	6.6	12.5	5.40
11.0	0.77	126	78	4.3	4.5	8.1	29.6	19.9	0.09	0.8	6.1	13.7	5.06
10.0	0.90	126	80	5.0	5.2	8.5	31.5	21.1	0.09	0.8	5.7	15.0	4.69
9.0	1.02	126	81	5.7	5.9	8.9	33.5	22.5	0.09	0.8	5.4	16.3	4.30
8.7	1.05	126	81	6.0	6.2	9.0	34.3	22.9	0.09	0.8	5.2	16.8	4.17
8.0	1.11	126	82	6.6	6.8	9.3	35.8	24.0	0.09	0.8	5.0	17.8	3.88
7.0	1.16	125	83	7.7	7.9	9.8	38.5	25.7	0.08	0.8	4.6	19.3	3.45
6.0	1.16	124	83	9.1	9.3	10.4	41.5	27.8	0.08	0.8	4.3	21.0	2.99
5.0	1.11	123	83	10.8	11.1	11.1	45.2	30.2	0.08	0.8	3.9	22.9	2.52
4.0	1.00	121	82	13.2	13.6	12.0	49.7	33.3	0.08	0.8	3.5	25.1	2.05
3.0	0.81	117	80	16.8	17.2	13.3	55.8	37.3	0.08	0.8	3.1	27.6	1.55
2.0	0.55	111	76	22.9	23.3	15.1	64.8	43.3	0.08	0.8	2.7	30.5	1.05
1.0	0.25	99	68	36.7	37.2	18.6	81.6	54.5	0.08	0.8	2.1	34.6	0.53

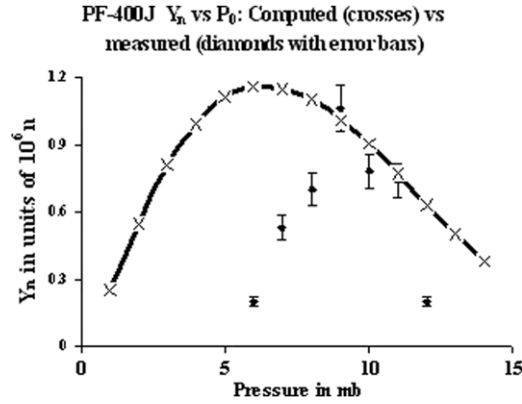


**Figure 2.** PF-400J: computed (crosses) compared with the measured [16] (diamonds with error bars)  $Y_n$  as functions of  $P_0$ . Vertical scale is in units of  $10^6$  neutrons per shot.

together with emission anisotropy data from which can be deduced the  $Y_n$  versus  $P_0$  curve. We first digitize the measured current derivative waveform [17] using an open access source digitizing program, Engauge [32] and then integrate the data with time to obtain the current waveform. Then we fit the computed current waveform to the published measured waveform as follows:

We configure the Lee model code to operate as the FN-II (electrode II) starting with the following published [17] bank and tube parameters:

- Bank parameters:  $L_0 = 54 \text{ nH}$ ,  $C_0 = 7.45 \text{ } \mu\text{F}$ ,  $r_0 = \text{not given}$
- Tube parameters:  $b = 5 \text{ cm}$ ,  $a = 2.5 \text{ cm}$ ,  $z_0 = 3 \text{ cm}$

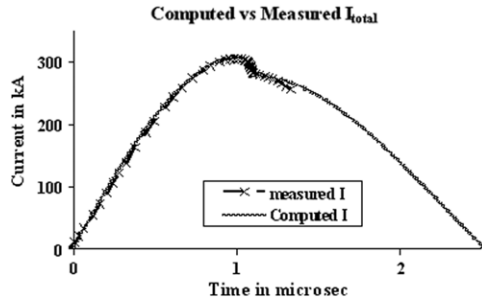


**Figure 3.** FN-II: computed discharge current compared with the published measured current [17] (derived) for FN-II. The measured discharge current is integrated to just beyond the bottom of the current dip, up to only  $1.4 \mu\text{s}$ .

Operating parameters:  $V_0 = 36 \text{ kV}$ ,  $P_0 = 2.75 \text{ Torr deuterium}$ .

To obtain a reasonably good fit the following bank and tube parameters ( $L_0$ ,  $C_0$  and  $z_0$  refitted and  $r_0$  fitted) are used:

Bank parameters:  $L_0 = 75 \text{ nH}$ ,  $C_0 = 7.45 \mu\text{F}$ ,  $r_0 = 10 \text{ m}\Omega$

Tube parameters:  $b = 5 \text{ cm}$ ,  $a = 2.5 \text{ cm}$ ,  $z_0 = 4 \text{ cm}$

Operating parameters:  $V_0 = 36 \text{ kV}$ ,  $P_0 = 2.75 \text{ Torr deuterium}$

together with the following fitted model parameters:

$$f_m = 0.12, \quad f_c = 0.7, \quad f_{mr} = 0.13 \quad \text{and} \quad f_{cr} = 0.7.$$

It can be seen that the computed discharge current waveform agrees well with the published measured current waveform up to and slightly beyond the bottom of the current dip (figure 3). This means that the agreement covers all the regions of interest from axial to radial phases up to the end of the pinch phase; all five plasma focus phases of interest to us.

#### 4.2. Computing the neutron yield as a function of operating pressure

Using the fitted model parameters, numerical experiments are then carried out at various initial pressures in deuterium. The neutron yields  $Y_n$  are then tabulated in table 2 and compared with the published measured values [17] in figure 4. The values of  $Y_n$  in table 2 are derived from the measured side-on differential yield per solid angle by multiplying each value by  $4\pi$  and 1.11 as suggested by the discussion of anisotropy in [17]. Using this method the optimum  $Y_n$  at 2.75 Torr attains a value of  $2.2 \times 10^8$  instead of the value of  $1.66 \times 10^8$  quoted by Castillo *et al* [17]. It appears that this difference is due to the different readings of the Ag counters in their two sets of measurements. To simplify matters we are actually presenting the results without taking into account this difference. That is, we are using a peak value of  $2.2 \times 10^8$  (using the multiplying factor suggested by the paper) instead of the peak value of  $1.66 \times 10^8$  which is quoted as the peak value of  $Y_n$ . This gives us a less degree of agreement than if we had adjusted the  $Y_n$  values so that the peak were  $1.66 \times 10^8$ . This way we are more conservative in claiming the degree of agreement.

Figure 4 shows that the computed neutron yield versus pressure curve agrees reasonably with the published curve. Features of comparison include peak  $Y_n$  (computed value of  $1.35 \times 10^8$  compared with the measured of  $2.2 \times 10^8$  which agrees to better than factor of 2), optimum  $P_0$  (computed value of 4 Torr compared with the measured value of 2.75 Torr)

**Table 2.** FN-II: Computed  $Y_n$  as a function of pressure, together with some computed pinch properties.  $I_{\text{peak}}$  is the peak value of the total current,  $I_{\text{pinch}}$  the plasma pinch current at start of pinch,  $T_{\text{pinch}}$  the pinch temperature,  $v_a$  the axial speed,  $v_s$ ,  $v_p$  the radial shock and piston speeds,  $r_{\text{min}}$  the minimum radius of focus,  $z_{\text{max}}$  the maximum length of pinch column, ‘Pinch dur’ the pinch duration,  $V_{\text{max}}$  the maximum induced voltage and  $n_i$  the ion number density.

$P_0$ (Torr)	$Y_n$ ( $10^8$ )	$I_{\text{peak}}$ (kA)	$I_{\text{pinch}}$ (kA)	Min $T_{\text{pinch}}$ ( $10^6$ )	Max $T_{\text{pinch}}$ ( $10^6$ )	Peak $v_a$ ( $\text{cm } \mu\text{s}^{-1}$ )	Peak $v_s$ ( $\text{cm } \mu\text{s}^{-1}$ )	Peak $v_p$ ( $\text{cm } \mu\text{s}^{-1}$ )	$r_{\text{min}}$ (cm)	$z_{\text{max}}$ (cm)	pinch dur (ns)	$V_{\text{max}}$ (kV)	$n_i$ ( $10^{23} \text{ m}^{-3}$ )
8.0	0.47	322	168	0.91	1.06	4.9	15.6	10.5	0.44	3.6	54.5	14.1	4.0
6.0	1.01	320	187	1.59	1.75	5.5	19.2	12.9	0.40	3.6	41.8	19.8	3.6
5.0	1.24	319	194	2.09	2.26	6.0	21.5	14.4	0.39	3.6	36.8	23.2	3.2
4.0	1.35	316	198	2.77	2.95	6.5	24.2	16.2	0.38	3.6	32.0	27.1	2.7
3.0	1.28	311	200	3.78	4.00	7.2	27.8	18.6	0.37	3.6	27.5	31.6	2.1
2.8	1.24	309	199	4.05	4.27	7.4	28.7	19.2	0.37	3.6	26.6	32.6	2.0
2.0	0.99	299	196	5.51	5.76	8.3	33.1	22.1	0.36	3.6	22.9	37.1	1.5
1.0	0.50	272	181	9.49	9.83	10.3	42.8	28.5	0.36	3.6	17.5	44.7	0.8

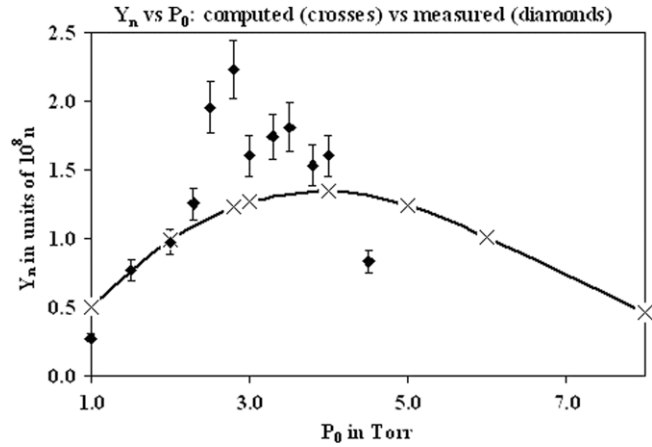


**Figure 4.** FN-II: computed compared with the measured [17]  $Y_n$  as functions of pressure. Vertical scale is in units of  $10^8$  neutrons per shot.

and the drop-off of  $Y_n$  on both sides of the optimum  $P_0$ , although the drop-off is more gradual for the computed curve than that for the measured curve.

The agreement between computed  $Y_n$  versus  $P_0$  data and measured  $Y_n$  versus  $P_0$  for each machine is even more remarkable when we note that model parameters are fitted by comparison of current traces; after fitting no more adjustments are done to any parameters. The same model code also shows reasonable agreement in neutron yield when compared with the published results of the PF1000 [3]; and it may be worthwhile to note that the PF-400 J is a small plasma focus of 400 J, the FN-II is 10 times bigger in storage energy, whilst the PF1000 is one of the biggest plasma focus in the world at 1 MJ. Thus the code computes realistic  $Y_n$  across practically the whole range of existing plasma focus devices.

Despite all the discussions in the literature [1, 2] about neutron production mechanisms such as beam–target, gyrating ions, moving boiler and others, the state of the art is not able to do better than make order of magnitude estimates, except in the case of thermonuclear models [7, 8], and those cases require parameters specifically adjusted to make the computed  $Y_n$  agree with the measured  $Y_n$ . On the other hand, our figures 2 and 4 are modeled with a more

acceptable beam–target mechanism using a more realistic code without adjusting parameters to fit the neutron yield to any specific machine.

## 5. Conclusion

The Lee model code is used to compute the neutron yield versus pressure curve of the Chilean PF-400 J and the Mexican FN-II. The computed results agree reasonably well with the published curves and give confidence that the Lee model code computes not just optimum neutron yields but also the behavior of neutron yield with pressure for specific plasma focus machines. The results indicate that this code, now incorporated with a beam–target mechanism, gives realistic plasma dynamics and focus properties together with a realistic neutron yield, applicable to a wide range of plasma focus devices, without the need of any adjustable parameters, needing only to fit the computed current trace to a measured current trace.

We may also remark that to do a better evaluation of any model for the mechanism of neutron production in plasma focus devices, it is necessary to use experimental diagnostics with high spatial and temporal resolution. Temporal and spatial resolution close to the pinch moment are crucial to describe properly the plasma heating. For example, to study radial velocities higher than  $20 \text{ cm } \mu\text{s}^{-1}$  ( $200 \text{ } \mu\text{m ns}^{-1}$ ) with optical refractive diagnostics requires shuttering pulses shorter than 100 ps; to obtain the necessary spatial resolution of  $20 \text{ } \mu\text{m}$  for the imploding on-axis shock front. Visible streak camera of sufficient time and space resolution could also be used to assess the radial velocity and the duration of the pinch. Experimental measurements of the ion density and temperature with temporal resolution of the order of nanoseconds are also required for devices in the range of sub-kilojoule to a few kilojoules.

## Acknowledgment

L Soto is supported by the Chile Bicentennial Program in Science and Technology grant ACT 26, Center of Research and Applications in Plasma Physics and Pulsed Power Technology (P<sup>4</sup>-Project).

## References

- [1] Bernard A, Bruzzone H, Choi P, Chuaqui H, Gribkov V, Herrera J, Hirano K, Krejci A, Lee S and Luo C 1998 *J. Moscow Phys. Soc.* **8** 93–170
- [2] Soto L 2005 *Plasma Phys. Control. Fusion* **47** A361
- [3] Gribkov V A *et al* 2007 *J. Phys. D: Appl. Phys.* **40** 3592
- [4] Moo S P, Chakrabarty C K and Lee S 1991 *IEEE Trans. Plasma Sci.* **19** 515
- [5] Springham S V, Lee S and Rafique M S 2000 *Plasma Phys. Control. Fusion* **42** 1023
- [6] Lerner E 2004 [arXiv:physics/0401126](https://arxiv.org/abs/physics/0401126)
- [7] Moreno C, Bruzzone H, Martínez J and Clausse A 2000 *IEEE Trans. Plasma Sci.* **28** 1735
- [8] González J H, Clausse A, Bruzzone H and Florido P C 2004 *IEEE Trans. Plasma Sci.* **32** 1383
- [9] Huba J D 2006 *Plasma Formulary* p 44 [http://wwwppd.nrl.navy.mil/nrlformulary/NRL\\_FORMULARY\\_07.pdf](http://wwwppd.nrl.navy.mil/nrlformulary/NRL_FORMULARY_07.pdf)
- [10] Lee S 1984 *Proc. 1983 College on Plasma Physics, ICTP (Trieste, Italy) Radiations in Plasmas* vol 2 ed B McNamara (Singapore: World Scientific) pp 978–87
- [11] Potter D E 1971 *Phys. Fluids* **14** 1911
- [12] Lee S 2000/2007 <http://ckplee.myplace.nie.edu.sg/plasmaphysics/>
- [13] Lee S 2005 ICTP Open Access Archive <http://eprints.ictp.it/85/>
- [14] Lee S and Saw S H 2008 *J. Fusion Energy* **27** 292–5
- [15] Lee S 2008 *Plasma Phys. Control. Fusion* **50** 105005
- [16] Silva P, Moreno J, Soto L, Birstein L, Mayer R E and Kies W 2003. *Appl. Phys. Lett.* **83** 3269
- [17] Castillo F, Herrera J J E, Rangel J, Alfaro A, Maza M A and Sakaguchi V 2002 *Braz. J. Phys.* **32** 3–12
- [18] Lee S *et al* 1988 *Am. J. Phys.* **56** 62

- [19] Tou T Y, Lee S and Kwek K H 1989 *IEEE Trans. Plasma Sci.* **17** 311
- [20] Lee S 1991 *IEEE Trans. Plasma Sci.* **19** 912
- [21] Lee S and Serban A 1996 *IEEE Trans. Plasma Sci.* **24** 1101–5
- [22] Ali J b 1990 Development and studies of a small plasma focus *PhD Thesis* Universiti Teknologi Malaysia, Malaysia
- [23] Liu M H, Feng X P, Springham S V and Lee S 1998 *IEEE Trans. Plasma Sci.* **26** 135–40
- [24] Lee S 1998 *Twelve years of UNU/ICTP PFF—a review IC*, 98 (231) Abdus Salam ICTP, Miramare, Trieste; ICTP OAA: <http://eprints.ictp.it/31/>
- [25] Lee S, Lee P, Zhang G, Feng X, Gribkov V A, Liu M, Serban A and Wong T 1998 *IEEE Trans. Plasma Sci.* **26** 1119
- [26] Bing S 2000 Plasma dynamics and x-ray emission of the plasma focus *PhD Thesis* NIE ICTP Open Access Archive <http://eprints.ictp.it/99/>
- [27] Siahpoush V, Tafreshi M A, Sobhanian S and Khorram S 2005 *Plasma Phys. Control. Fusion* **47** 1065
- [28] Lee S *Radiative Dense Plasma Focus Computation Package: RADPF* <http://www.intimal.edu.my/school/fas/UFLF/>; <http://www.plasmafocus.net/IPFS/modelpackage/File1RADPF.htm>
- [29] Lee S, Saw S H, Lee P C K, Rawat R S and Schmidt H 2008 *Appl. Phys. Lett.* **92** 111501
- [30] Lee S, Lee P, Saw S H and Rawat R S 2008 *Plasma Phys. Control. Fusion* **50** 065012
- [31] Lee S and Saw S H 2008 *Appl. Phys. Lett.* **92** 021503
- [32] 2009 [http://sourceforge.net/project/showfiles.php?group\\_id=67696&package\\_id=130007&release\\_id=500277](http://sourceforge.net/project/showfiles.php?group_id=67696&package_id=130007&release_id=500277)